

3 Experimental methods

3.1 Thermogravimetry coupled with mass spectrometry (TGA-MS)

The apparatus includes a STA409 thermal analyzer from Netzsch coupled with a quadrupole mass spectrometer Quadstar 422 from Balzers (Fig. 3.6). A typical measurement is done at 1 bar in a flow of an inert gas (argon, 250 ml/min). The sample is heated successively and the weight loss is measured with a precision < 1 mg. A fraction of the evolving gases is analyzed with the mass spectrometer. At the top of the oven, a small hole connects the sample chamber

($p = 1013$ mbar) to the fore-vacuum chamber ($p \approx 1$ mbar). The fore-vacuum chamber is connected to the mass spectrometer by a ceramic skimmer with a hole of $10 \mu\text{m}$ diameter. The pressure inside the mass spectrometer was $4 \cdot 10^{-6}$ mbar for all measurements.

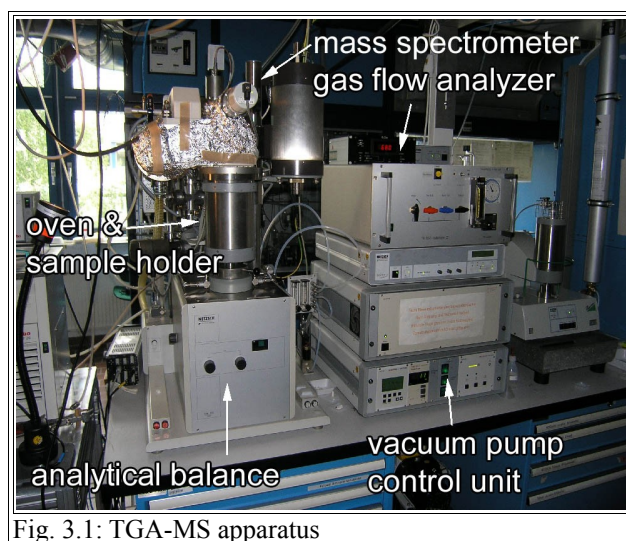


Fig. 3.1: TGA-MS apparatus

3.2 Scanning microscope for semiconductor characterization

The scanning microscope for semiconductor characterization (SMSC) allows the space-resolved imaging of photocurrents (Fig. 3.1 and 3.3). A red HeNe-Laser ($\lambda = 632.8 \text{ nm}$) is directed through an inverse microscope and illuminates the sample with a spot diameter between $10 - 400 \mu\text{m}$. The table of the microscope can be moved in x- and y-direction with a resolution of $100 \mu\text{m}$. Since the photocurrent is typically very small in the range of a few nanoampere, the Laser-spot is modulated with a mechanic chopper and amplified with a lock-in amplifier. The chopper frequency was 15 Hz if not stated otherwise. The light intensity can be adjusted by neutral gray filters and was between 10 mWcm^{-2} and 100 mWcm^{-2} for most measurements. A detailed introduction is given in [123].

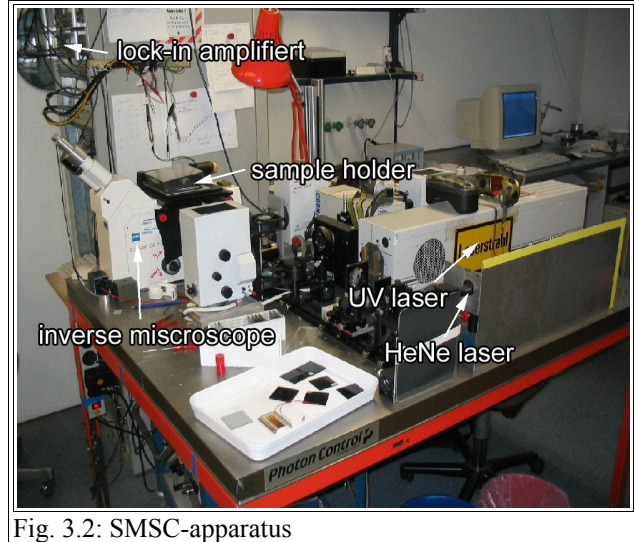


Fig. 3.2: SMSC-apparatus

The photocurrent is typically very small in the range of a few nanoampere, the Laser-spot is modulated with a mechanic chopper and amplified with a lock-in amplifier. The chopper frequency was 15 Hz if not stated otherwise. The light intensity can be adjusted by neutral gray filters and was between 10 mWcm^{-2} and 100 mWcm^{-2} for most measurements. A detailed introduction is given in [123].

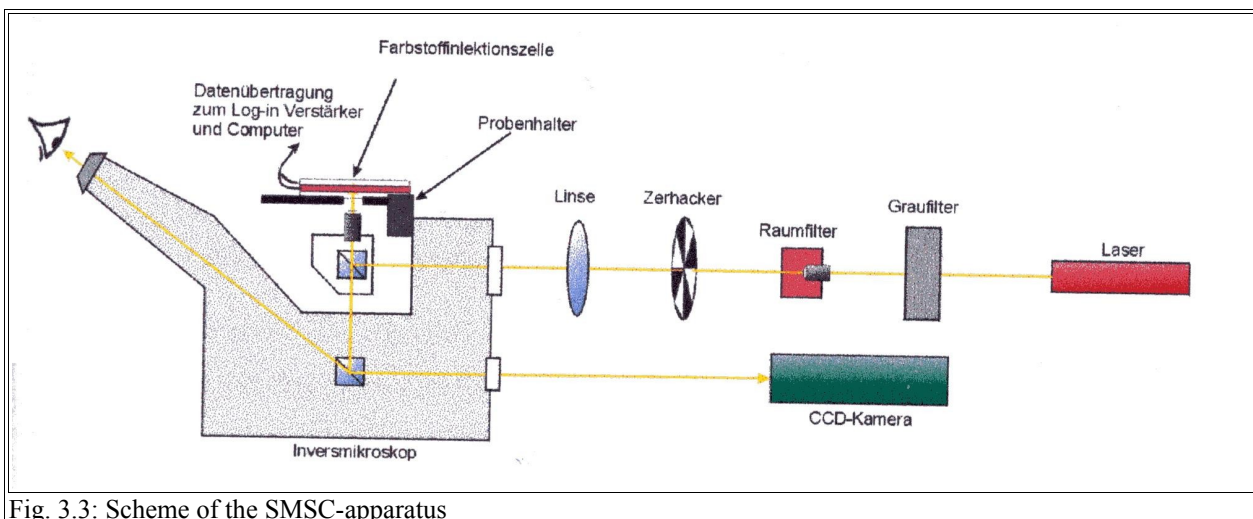


Fig. 3.3: Scheme of the SMSC-apparatus

3.3 Scanning electron microscopy (SEM)

Scanning electron microscopy (SEM) images were recorded with a field emission microscope LEO1530 (Gemini) (Fig. 3.4). At an electron energy of 20 keV, it has a maximum resolution of 1 nm, at 1 keV of about 3 nm. The minimal distance between the sample and the detector lens is 1 mm. Besides the standard secondary electron detector, it is equipped with an energy dispersive X-ray spectrometer for elementary analysis (EDX).

If not stated otherwise the pictures in this study were made at 2 keV.



Fig. 3.4: Field emission microscope LEO1530 (Gemini)

3.4 Transient photovoltage/photocurrent measurements

A detailed description of the apparatus is given in chapter 6.2.2. Briefly, a solid state switch was used to operate a LED-ring module from Luxeon both with a constant bias illumination and a short light pulse of a few microseconds (Fig. 3.5). The pulse was given by a pulse generator TGP110 from TTI. The pulse length could be adjusted between 50 ns - 5 s, the pulse amplitude between 0.1 V and 10 V and the repetition rate between 0.1 Hz and 10 Mhz.

The voltage of the illuminated solar cell as a function of time was recorded with a storage oscilloscope USB Scope 1 Mephisto UM 202 from Meilhaus Elektronik. This scope had two channels with a maximum resolution of 16 bits for an input voltage between ± 100 mV and ± 10 V. The internal memory was 256 ks. The maximum time resolution was 1 μ s.

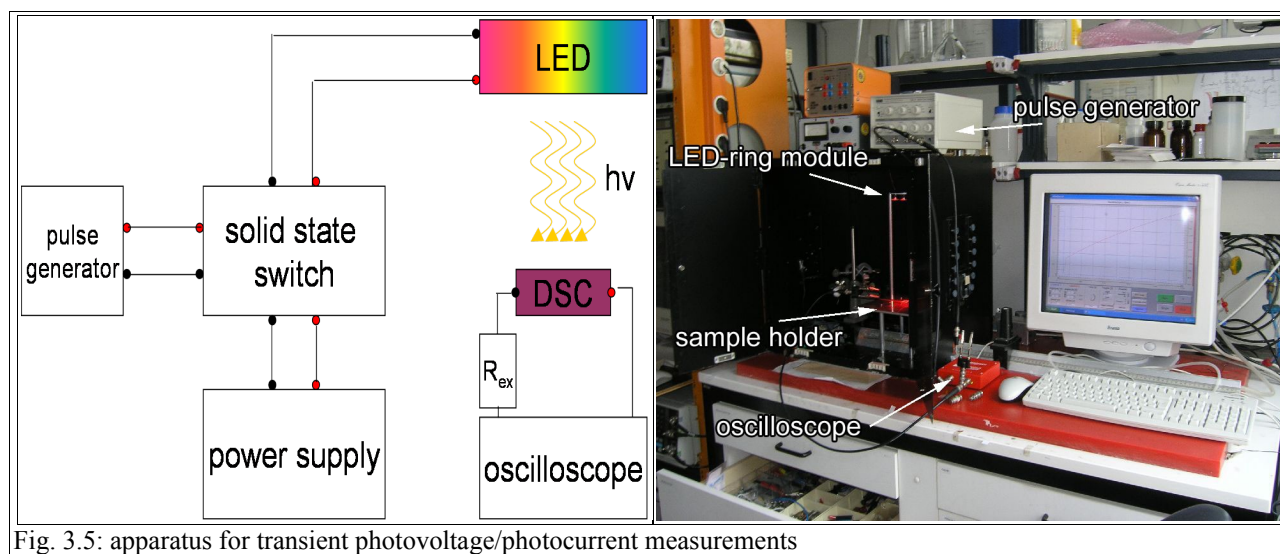


Fig. 3.5: apparatus for transient photovoltage/photocurrent measurements

3.6 Step profilometer

For the measurement of layer thicknesses (FTO, TiO₂, carbon, ...) a DEKTAK 8 Advanced Development Profiler from Veeco (Fig. 3.7) was used. It measures the vertical displacement of the diamond tipped stylus electromechanically. The gantry moves the stylus according to an user-programmed scan length, speed and stylus force. The stylus has a diameter of 25 μm . The vertical resolution varies between 0.1 nm (maximum layer thickness 6.5 μm) and 4 nm (max. 262 μm). For all measurements the stylus force was 7.5 mg.

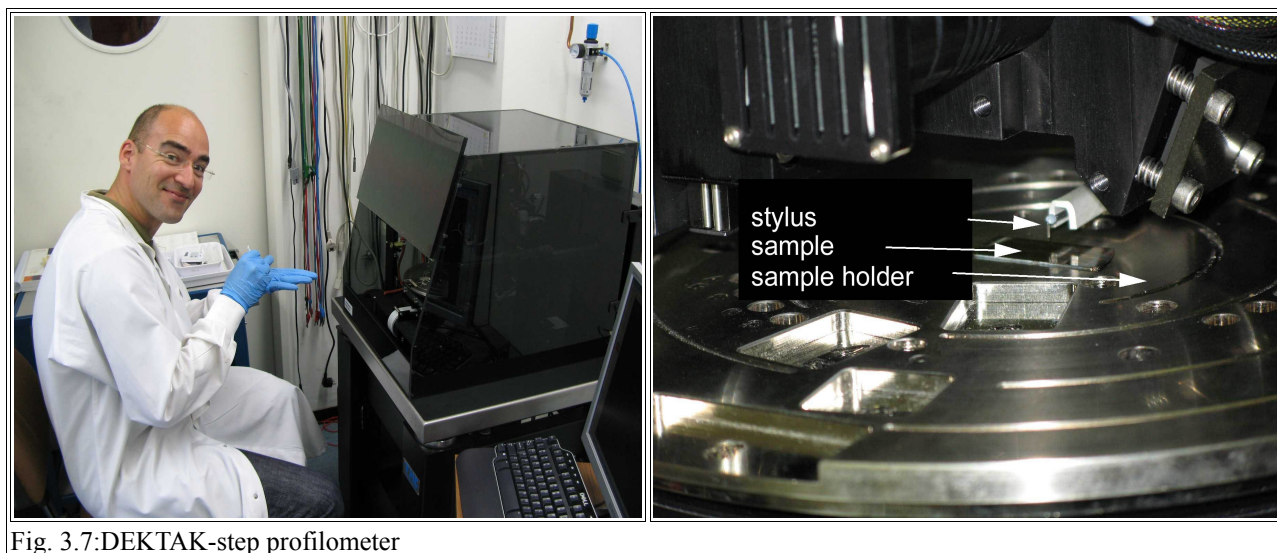


Fig. 3.7:DEKTAK-step profilometer

3.7 Current-Voltage-curves

3.7.1 Experimental setup

Current-voltage-curves (I-V-curves) shown in chapter 6.4 (Nano surface conductivity solar cell) were recorded with an EG&G Model A273 potentiostat. Cyclic voltammograms were recorded going from 0.1 V (reverse bias) to -0.9 V (forward bias) with a scan rate of 50 mVs^{-1} if not stated otherwise. Two cycles were made for each measurement. If the second cycles deviated more than 5 % from the first one, more cycles were recorded until the system reached a steady state.

For the measurement of nano-surface conductivity cells (NSCSC) it happened that a hysteresis was seen for the back and forth scan respectively. Then it was tried to slow down the scan rate (up to 10 mVs^{-1}) and if this scan rate was still too fast the average of back and forth scan was taken to estimate the solar cell efficiency.

The light source were LED-ring modules of different wavelength. The spectra are shown in Fig. 3.8.

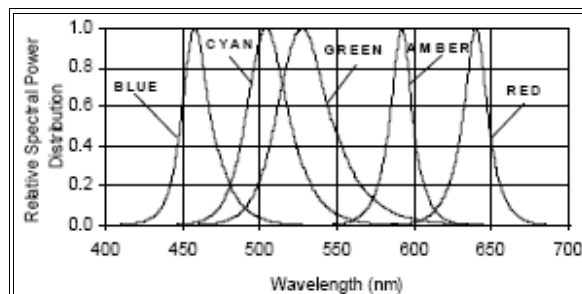


Fig. 3.8: spectra of LED ring modules taken from Luxeon technical data sheet DS22

The light intensity was adjusted so that the photon flux I_{ph} correspond to the photon flux of the AM1.5 spectrum with a threshold wavelength of 660 nm.

$$I_{ph} = \int_0^{660} I_{ph}(\lambda) d\lambda = 1.09 * 10^{17} \text{ s}^{-1} \text{ cm}^{-2} \quad (3.1)$$

The underlying idea is that photons with a wavelength > 660 nm are not absorbed by the dye anymore and do not contribute to the photocurrent. Calibration measurements were done with a photodiode with a known spectral response (details given in chapter 6.2.2). In other words the number of photons absorbed by the dye was the same for the LED-ring as for an AM1.5 spectrum, however the penetration depth differed. The latter might have an influence on the conversion efficiency especially if the electron transport with the layer is hindered and/or the recombination rate is high.

To summarize I-V-curves shown in chapter 6.3 and 6.4 where not recorded with a standard AM1.5 spectrum but with LEDs, which emit the same number of absorbed photons as an AM1.5 spectrum.

I-V-curves shown in chapter 6.5 (Accelerated aging tests on dye sensitized solar cells) were recorded with a Keithley 2400 Source Meter and a Steuernagel solar simulator. The light intensity was 100 mWcm^{-2} and the scan rate 100 mVs^{-1} if not stated otherwise. The measurement mode was from short circuit current to open circuit potential. No hysteresis was seen if the cells were measured back and forth.

For all experiments the cells were covered with a mask that was slightly bigger than the active cell area. This ensures that most of the diffusive light is captured by the cell, but additional photons that are trapped by the glass and transferred to the cell by multiple reflection are absorbed by the mask. This is believed to be the most accurate method to determine the solar cell parameters [124].

3.7.2 Analysis of Current-Voltage-curves

The four most fundamental parameters extracted from an I-V-curve of a given solar cell are (Fig. 3.9):

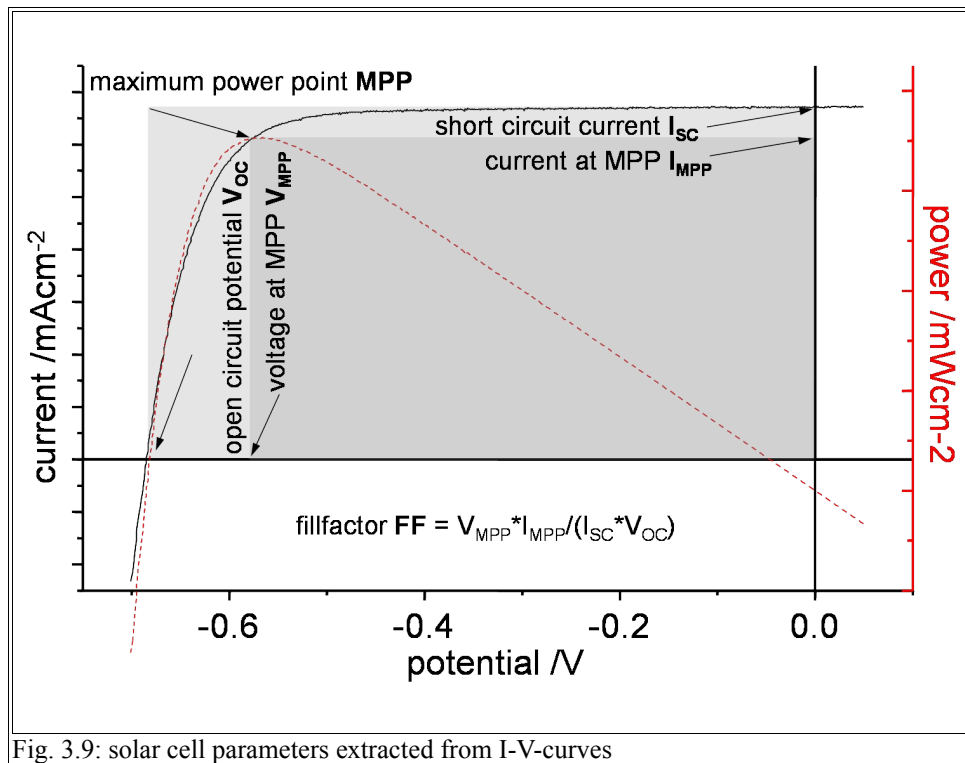


Fig. 3.9: solar cell parameters extracted from I-V-curves

- 1) **efficiency η** : the ratio between the maximum power point MPP of a solar cell and the power of the incoming radiation

$$\eta = \frac{I_{MPP} * V_{MPP}}{\int_0^{\infty} h\nu I_{ph}(h\nu)} \quad (3.2)$$

- 2) **open circuit potential V_{OC}** : the potential of the solar cell if no current flows
- 3) **short circuit current I_{SC}** : the current of the solar cell if no potential is applied
- 4) **FF**: the ratio between the maximum power and the product of the short circuit current and the open circuit potential

$$\eta = \frac{I_{MPP} * V_{MPP}}{I_{SC} * V_{OC}} \quad (3.3)$$

Other solar cell parameters can be extracted from the I-V-curve by modeling. The most commonly applied model, the so-called two diode model, is based on the assumption that the solar cell behaves like an ideal diode. A equivalent circuit is given in Fig. 3.10.

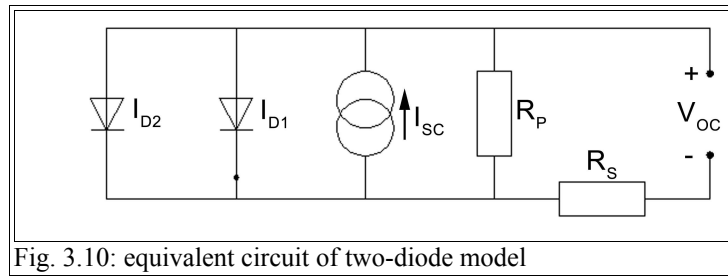


Fig. 3.10: equivalent circuit of two-diode model

It is based on the assumption that diode 1 and diode 2 with the currents I_{D1} and I_{D2} behave like ideal diodes and can be described by the fundamental equation first derived by *Shockley* [125]

$$I_{Dx} = I_{Sx} * \left(e^{\frac{U}{nx * U_T}} - 1 \right) \quad (3.4)$$

For a given semiconductor the saturation current I_{S1} is proportional to the thermally induced recombination/generation processes of charge carriers. I_{S1} increases exponentially with increasing temperature. At room temperature I_{S1} is in the range of 1 - 10 pA for silicon solar cells (details are given in chapter 6.1). However, in real devices the saturation current I_S is found to be about three orders of magnitudes higher, which is due to non-irradiative recombination/generation processes of charge carriers at trap states. That is why a second diode is introduced with a saturation current I_{S2} . The ideality factor $n1$ is normally set to be one and $n2$ can typically varies between one and two. The ideality factor $n2$ gives an idea about the position of the trap states in conventional p/n solar cells. If $n2$ is close to one and temperature independent, there are shallow trap states with a narrow energy distribution. If the trap states come closer to the middle of the bandgap, $n2$ approaches two and if the trap states are not localized and distributed all over the bandgap, $n2$ correlates with the temperature.

In this simple model the photogenerated charge carriers are described by the short circuit current I_{SC} , which flows as an offset in the opposite direction. Finally all series resistance are summarized by R_S and all parallel resistance by R_P . Thus the photocurrent I_Q can be calculated as

$$I_Q = I_{S1} * \left(e^{\frac{U - I_Q * R_S}{U_T}} - 1 \right) + I_{S2} * \left(e^{\frac{U - I_Q * R_S}{2U_T}} - 1 \right) + I_{SC} + \frac{U - I_Q * R_S}{R_P} \quad (3.5)$$

In most solar cells it is imperative that $R_P \gg R_S$ (in an ideal solar cell $R_P = \infty$ and $R_S = 0$). Under this assumption equation 3.5 simplifies at $U \rightarrow 0$

$$R_P = \left(\frac{\delta U}{\delta I} \right)_{U \rightarrow 0} \quad (3.6)$$

and $U \rightarrow V_{OC}$

$$R_S = \left(\frac{\delta U}{\delta I} \right)_{U \rightarrow V_{OC}} \quad (3.7)$$

That means the sum of all series resistance can be easily identified as the slope of the I-V-curve at V_{OC} and the sum of all ohmic parallel resistance as the slope of the I-V-curve at I_{SC} (Fig. 3.9).

By measuring the dark curve of a solar cells, one can also get an idea of the saturation current I_0 . At $V \rightarrow 0$ the current is mostly determined by the parallel resistance, then there is a branch where the device behaves like an ideal diode and once the internal electric field diminishes the current is determined by the sum of all series resistance of the cell. Plotting the I-V-curve in a semi-logarithmic scale ($\ln I$ vs. U) the exponential part becomes a straight line and extrapolating the line to the interception with the y-axis gives the saturation current I_0 .

The question arises if equation 3.4 and 3.5 can also be applied to dye sensitized solar cells (DSSCs) and what is the meaning of I_{Sx} in these kinetically controlled devices? In DSSCs, titaniumdioxide with a bandgap > 3 eV is the semiconductor and according to equation 3.4 I_S would only be in the range of 10^{-43} Acm⁻². Yet measuring I_S for a standard DSSC, it is found to be in the range of 1nA-1μA. Obviously I_S is controlled by the exchange current at the FTO/electrolyte interface. This can

be demonstrated if small amounts of Pt are deposited on FTO front electrode [126]. Then the exchange current increases by several orders of magnitude and the rectifying properties of device diminish. Thus the saturation current in DSSCs depends on the rate constant of the triiodide reduction and is a kinetic parameter whereas in silicon solar cells it is a thermodynamic parameter. Furthermore equation 3.4 was derived for single bandgap semiconductors where the electric properties are mainly governed by the bandgap and only few trap states are present. In DSSC, nanoporous titanium dioxide with a huge surface area of about $50 \text{ m}^2\text{g}^{-1}$ is used, and the electric properties are governed by subband gap states. It is believed that there is an exponential trapstate distribution below the conduction band edge [15]. The electron transport and thus the conductivity is almost exclusively determined by this trap state distribution and not by the position of the conduction band edge. To summarize equation 3.4 is based on assumptions that are not applicable for DSSC. Yet, the I-V-curve of a standard DSSC can be well fitted with the two diode model and it is an useful method to learn about the parallel and series resistance.